ORIGINAL PAPER

Structure and properties of electrodeposited Ni–Co–YZA composite coatings

**Meenu Srivastava · V. K. William Grips ·
K. S. Rajam**

Abstract The aim is to develop an economical composite coating with high thermal stability. Ni–Co alloys are found to possess better thermal, physical and mechanical properties compared to Ni. Also, oxide particles as distributed phase can impart better thermal stability. Hence, particulates of composite Yttria stabilised zirconia, a commonly used high temperature material and alumina (YZA) were reinforced in various Ni–Co alloy matrices through electrodeposition. The influence of YZA on the microhardness, tribology and corrosion behaviour of Ni–Co alloys with Co contents of 0 wt.%, 17 wt.%, 38 wt.% and 85 wt.% was evaluated. Optical and Scanning Electron Microscopy (SEM) confirmed the presence of YZA particles and Energy Dispersive X-ray Analysis (EDX) revealed the composition. Tribology testing showed that composite containing 38 wt.% Co displayed better wear resistance. It was found from the immersion corrosion studies that Ni–17Co–YZA coating displayed improved corrosion resistance. Thermal stability studies showed that Ni–85Co–YZA coating retained its microhardness at temperatures of 600 °C. Thus, these coatings can be tailored for various applications by varying the cobalt content.

Keywords Ni–Co · Composite · Yttria stabilised zirconia/alumina (YZA) · Wear · Immersion corrosion · Thermal stability

1 Introduction

Composite electroplating is a method of co-depositing insoluble particles of metallic or non-metallic compounds with metal or alloy, to improve the mechanical properties. Ni, Cu, Cr, Fe, Co, Ag and Au are the mainly used metal matrices and the distributed phase comprises particulates of metals, metal oxides, carbides, borides, nitrides and polymers. Oxides are preferred for high temperature applications due to their resistance/inertness to oxidation [1]. The commonly employed oxide reinforcements are Al_2O_3, SiO_2, Cr_2O_3, TiO_2, ZrO_2, partially stabilized zirconia (PSZ), CeO_2, La_2O_3 etc. Composites containing Al_2O_3, SiO_2, TiO_2 and Cr_2O_3 as reinforcements have been extensively studied, while the others are gaining importance [1–13]. In recent years there has been an increased interest in Ni–ZrO_2 composites [14–18]. ZrO_2 can be stabilised by the addition of various stabilizers such as yttria or ceria, thereby making them suitable for diverse applications [19]. A considerable number of literature studies cite the electrodeposition of PSZ with Ni and Co matrices [19–22]. Yttria stabilized zirconia (YSZ) is used in thermal barrier coatings (TBC) and also as an electrolyte in solid oxide fuel cells (SOFC). This is because of its high oxygen ion conductivity, stability in both oxidizing and reducing environments [23, 24]. However, it is brittle and susceptible to fracture. In addition, it exhibits low thermal conductivity, high thermal-expansion coefficient and low fracture toughness. The strength, toughness, thermal shock and corrosion resistance of YSZ can be improved by the addition of alumina [23, 25]. Alumina has also been used effectively as a pinning agent to reduce the dynamic grain growth and impart superplasticity during high temperature deformation of YSZ [24]. These composite coatings have been deposited by Air Plasma Spray (APS), Electron Beam

M. Srivastava (✉) · V. K. W. Grips · K. S. Rajam
Surface Engineering Division, National Aerospace Laboratories,
Post Bag No.1779, Bangalore 560017, India
e-mail: meenu_srivas@yahoo.co.uk

Physical Vapour Deposition (EBPVD) or processed through Powder Metallurgy route. These processes are not economical and hence, there is a growing demand to develop high temperature coatings by cost-effective routes. Lu et al. [26] have made an attempt to deposit YSZ/Al$_2$O$_3$ composite coatings by electrophoresis followed by sintering, to suit the high temperature applications.

In the present study, combustion synthesised YZA composite particulates were reinforced in Ni–Co alloy matrix via electrodeposition. Ni–Co was chosen as it is reported to have improved high temperature properties [27, 28], making it a potential matrix for high temperature applications. Ni–Co alloy deposition is of anomalous type, wherein the less noble metal Co deposits preferentially over the nobler metal Ni [29–39]. The present work was aimed at studying the structure, mechanical and chemical behaviour of the Ni–Co–YZA system. Tribological, corrosion and thermal stability studies of these composite coatings are included.

2 Experimental

2.1 Preparation and characterization of composite coating

Ni–Co–YZA composite coatings were electrodeposited employing nickel sulphamate bath of the following composition: 275 kg m^{-3} nickel sulphamate, 6 kg m^{-3} nickel chloride, 30 kg m^{-3} boric acid and 0.2 kg m^{-3} sodium dodecylsulphate. The cobalt content was varied from 1–28 kg m^{-3} as cobalt sulphamate so as to obtain 17 wt.%, 38 wt.% and 85 wt.% Co content in the coatings. The deposition was carried out under optimized conditions with YZA content of 25 kg m^{-3}, pH 4.0 and current density 7.75 mA cm^{-2}. The plating bath was maintained at ambient condition ≈ 30 °C. The YZA particles were kept in suspension in the electrolyte by magnetic stirring for a time period of 16 h prior to electrodeposition. The particles were in a dispersed condition during the deposition, by magnetic stirring at a speed of 200 rpm. The deposition was carried out on a brass substrate 0.0254 m × 0.0254 m, under galvanostatic conditions, so as to obtain a coating of thickness 50 ± 2 µm. The pretreatment conditions employed for the brass substrate are mentioned in detail in [40]. The nature and distribution of YZA particles in the composite coatings were studied using an optical microscope and SEM Leo 440I. The surface composition of the coatings was determined using EDX which was coupled with SEM. The YZA content across the cross-section was determined by image analysis technique, using the VE-DIOPRO 32 software supplied by M/s Leading Edge, Australia and is expressed as area fraction. The

microhardness of the composite coatings was measured on the cross-section using a Buehler microhardness tester (Micromet 2103) by employing a load of 50 gf. An average of five measurements is reported. The crystallinity and phase identification was done using a Rigaku X-ray diffractometer operated with CuK$_\alpha$ radiation. The average crystallite size was determined using the Debye–Scherrer equation [41].

2.2 Tribology testing

The tribological behaviour of the coatings was investigated by performing wear tests on a Pin-on-Disc tribometer (DUCOM, India). The detailed test conditions are discussed elsewhere [42]. The wear coefficient was calculated using the Archard relationship [43], which is valid for adhesive and abrasive wear. The Raman spectra of the wear tracks, on the disc of various Ni–Co–YZA composites were recorded with a DILOR-JOBIN-YVON-SPEX (Paris, France) integrated Raman Spectrometer (Model Labram). This investigation was done to identify the nature of products formed during tribo-testing.

2.3 Corrosion studies

The corrosion behaviour of the coatings was studied by employing the immersion corrosion technique. The composite coatings were electroformed on an Al substrate. An Al foil 0.0508 m × 0.0254 m × 0.001 m was chosen as the cathode and nickel sheet 0.1016 m × 0.0254 m was selected as the anode. The Al foil was subjected to a sequence of treatment procedures in accordance with ASTM B253-87 prior to deposition. The treated substrate was subjected to electrodeposition under the optimized conditions mentioned in 2.1. The electroplated Al foil was immersed in 4% NaOH solution for the dissolution of the Al substrate. The thus obtained composite electroforms were weighed and immersed in a corrosive medium of 3.5% NaCl (pH 5.5) for a duration of 168 h. After immersion they were ultrasonically cleaned, thoroughly dried and the weight was recorded. The corrosion rate was obtained using the weight loss method.

2.4 Thermal stability

The thermal stability of the composites was studied by heat treating the composite electroforms at temperatures of 200 °C, 300 °C, 400 °C and 600 °C in an electric furnace under atmospheric conditions, for 1 h. After the completion of heat treatment, electroforms were allowed to cool in

the furnace atmosphere. The heat treated composite electroforms were cut across the cross-section using a Buehler Isomet cutting machine. The cut samples were metallographically mounted (using Bakelite powder) and ground, polished (alumina slurry) employing a Buehler Ecomet grinder/polisher. The polished surface was subjected to microhardness testing using the Buehler Microhardness tester (Micromet 2103) employing a load of 50 gf.

3 Results and discussion

3.1 Microstructure

The as-synthesised YZA particulates shown in Fig. 1a were found to be alumina rich, varying in size (1–20 μm) and with platelet like appearance. The surface morphology of plain Ni coating (Fig. 2a) appeared as irregular polyhedral crystallites of varying size. However, the Ni–YZA composite displayed a matrix comprising of small irregular crystallites with no distinct boundaries, dispersed with YZA particles of varying shape and size (Fig. 2b). A change in the shape of the particles was also confirmed from optical micrographs, (insert in Fig. 2b). The EDX analysis of few of the incorporated particles mentioned in Table 1 show a variation in the composition. The cause for this change needs further understanding.
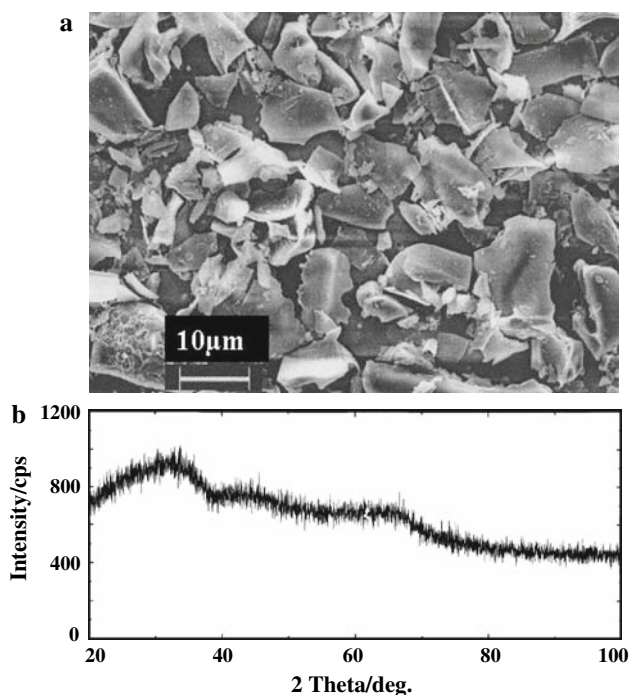
Fig. 1 SEM (**a**) and XRD diffractogram (**b**) of as-synthesized YZA powder
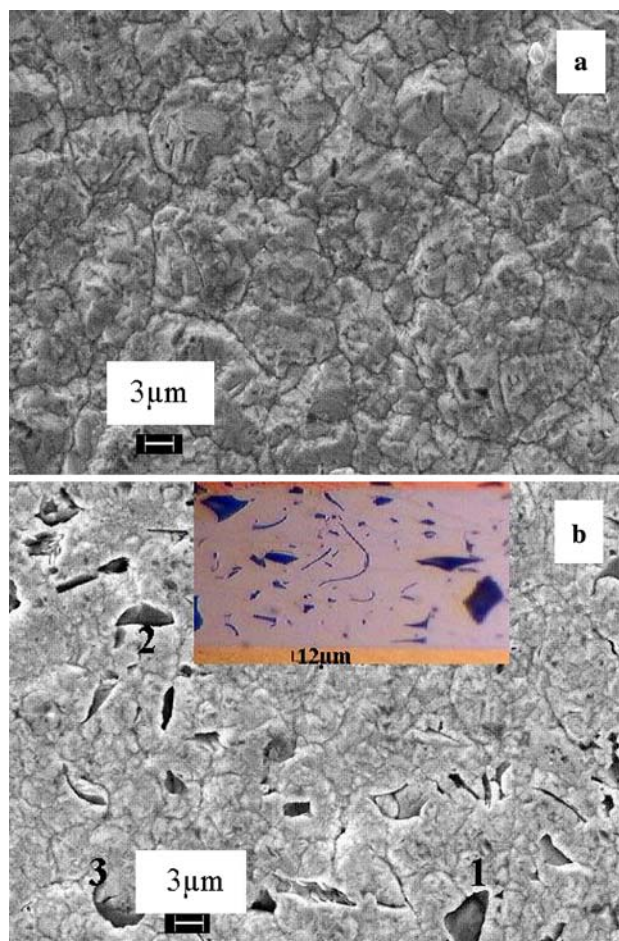
Fig. 2 Surface morphology of plain Ni (**a**) and Ni–YZA composite (**b**) coatings

Ni–Co alloys acquire different morphologies with change in the cobalt content [29, 40]. The effect of YZA on the surface morphology of various Ni–Co alloys is shown in Fig. 3. The constituents of few incorporated particles are mentioned in Table 1. On comparing Figs. 2b and 3a it was found that the addition of 17 wt.% Co to the Ni–YZA composite did not alter the surface morphology. A similar observation has been reported elsewhere for Ni–Co alloys [40]. This implies that the presence of YZA does not seem to influence the morphology of the alloy. EDX analysis revealed that irregular shaped YZA particles (1 and 2) were rich in zirconia, while filamental particles (3) were rich in alumina (Table 1). The surface morphology of Ni–38Co–YZA composite displayed in Fig. 3b shows alumina rich filamental and flaky YZA particles in a nodular grained matrix. A change in morphology is observed, compared to Ni–YZA and Ni–17Co–YZA composite coatings. The surface morphology of Ni–85Co–YZA composite coating, consisting of ridged grains of various sizes, straight, bent and gathered in thick bundles is shown in Fig. 3c. The blocky particles incorporated in the matrix were found to

Table 1 EDX analyses of some YZA particles incorporated in Ni–YZA, Ni–17Co–YZA, Ni–38Co–YZA and Ni–85Co–YZA composite coatings

Element	Ni–YZA (wt.%)			Ni–17Co–YZA (wt.%)			Ni–38Co–YZA (wt.%)			Ni–85Co–YZA (wt.%)			
	1_p	2_p	3_p	1_p	2_p	3_p	1_p	2_p	3_p	1_p	2_p	3_p	4_p
O	19	24	9	9	20	16	5	11	1	6	12	44	29
Al	6	5	1	1	3	13	4	6	<1	1	8	13	2
Co	–	–	–	12	7	9	33	29	38	81	67	18	49
Ni	70	55	88	77	52	54	57	50	61	8	8	3	5
Y	1	3	<1	<1	3	1	<1	1	<1	1	1	3	2
Zr	4	13	3	2	16	6	2	3	<1	3	5	20	13

p refers to particle

be rich in zirconia (Table 1). A similar morphology has been reported for plain cobalt electrodeposited coating [28]. Thus, it can be inferred that the change in matrix morphology is due to the influence of Co and not the YZA particles.

3.2 X-ray studies

It is clear from Fig. 1b that the YZA particulates are amorphous in nature. It is also evident from the diffractogram (Fig. 4) that composites with a Co content of 0 wt.% and 17 wt.% possessed fcc crystal structure and exhibited predominant (200) reflection along with the presence of a (111) line. Weak (220), (311) and (222) reflections are also observed. However, a predominant (111) reflection has been observed for Ni–38Co–YZA composite along with (220), (200), (311) and (222) reflections. Ni–85Co–YZA composite is found to possess an hcp crystal structure with predominant (100) and (110) reflections. (101), (200) and (201) reflections corresponding to hcp Co are also visible. No significant difference in the reflection lines is observed for Ni–17Co, Ni–38Co and Ni–85Co alloys (Fig. 4c (insert) and [40]). In the diffractograms of all the composites no other crystalline peaks are visible, confirming the amorphous nature of the YZA particles. Thus, it can be concluded that the incorporation of YZA did not transform the structure of Ni–Co alloys. The crystallite size in reference to (200) reflection was determined to be 23 nm for Ni–YZA composite. No variation in the size was observed for Ni–17Co alloy and the composite. A similar observation has been reported by Moller during the incorporation of ZrO₂ in Ni matrix [15]. However, alloying of Ni with 38 wt.% Co reduced the crystallite size to 16 nm. Also, a reduction in size to 12 nm was observed on the incorporation of YZA particles in Ni–38Co alloy matrix. An increase in crystallite size to 23 nm (reference to (100) reflection) was observed on the incorporation of YZA particulates in Ni–85Co matrix. This enhancement in size

compared to 38 wt.% Co composite can be associated to the hcp structure [40]. However, no change in size was observed compared to Ni–85Co alloy. This shows that YZA incorporation affects the crystallinity for a Co content of 38 wt.%.
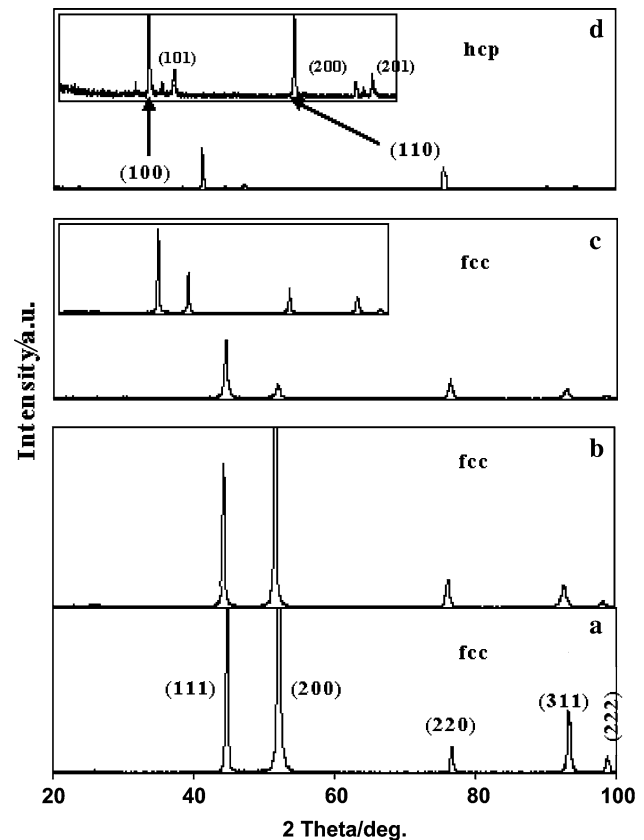
3.3 Microhardness

The anomalous Ni–Co alloy deposition is depicted in Fig. 5a. The effect of Co content in the deposit on the microhardness of Ni–Co alloys and their YZA composites is displayed in Fig. 5b. It is apparent that the hardness attained a maximum for a cobalt content of 38 wt.% with or without YZA particles. The maximum hardness can be associated with the optimum cobalt content required for the enhanced mechanical properties [45, 46]. The initial rise in hardness is associated with the fcc crystal structure possessed by Ni–17Co and Ni–38Co alloys. The reduced hardness of Ni–85Co alloy is due to the presence of the hcp phase [29, 40].

The microhardness of the composites can also be correlated with the extent of incorporation of YZA particles, expressed as area fraction in Table 2. The enhanced hardness of Ni–YZA (450 VHN) and Ni–17Co–YZA (460 VHN) composite coatings in comparison with the alloys (Plain Ni 260 VHN, Ni–17Co 395 VHN), is due to the contribution from the particle strengthening mechanism [47]. The contribution from Hall-Petch strengthening [48] appears to be nil, as no change in the crystallite size was observed with reference to the respective alloys (23 nm for plain Ni, Ni–17Co). However, the hardness of Ni–38Co–YZA (490 VHN) composite can be attributed to the contribution from Hall-Petch strengthening (crystallite size reduced from 16 nm to 12 nm) and particle strengthening. The Hall-Petch strengthening is due to two effects: firstly due to alloying of Ni with 38 wt.% Co (crystallite size reduces from 23 nm to 16 nm) and secondly due to the codeposition of YZA particles (size reduces from 16 nm
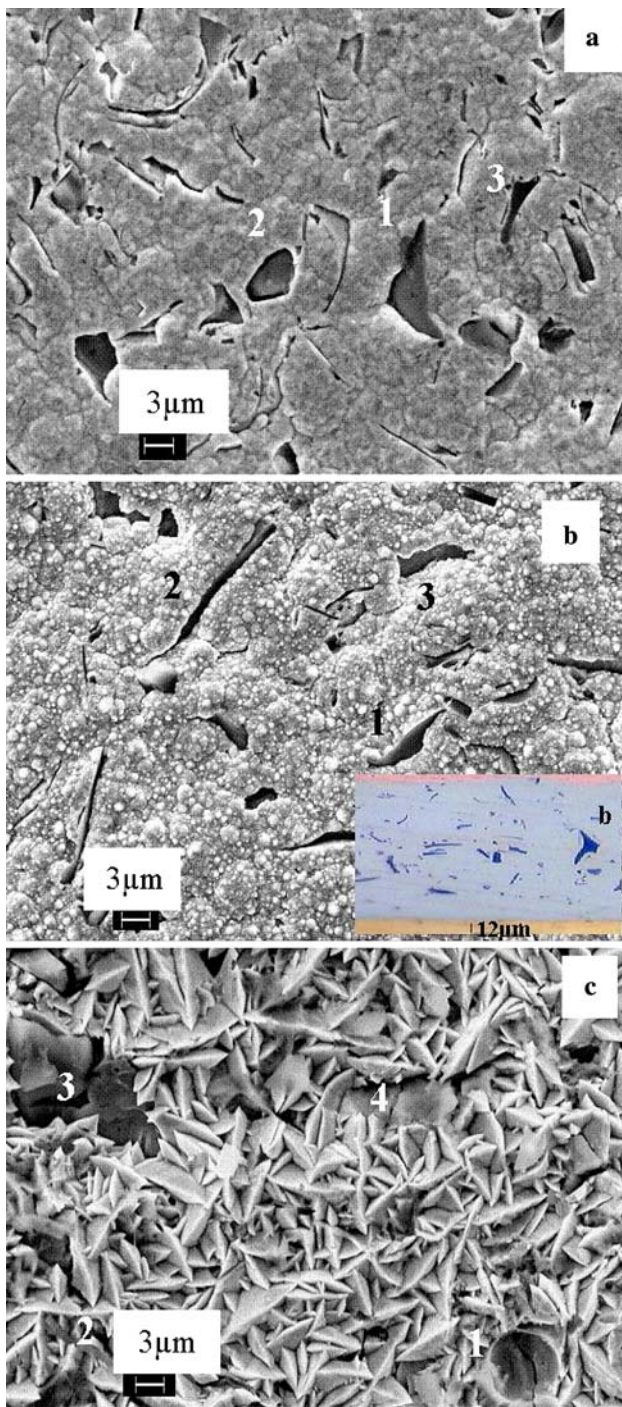
Fig. 3 Surface morphology of Ni–17Co–YZA (**a**), Ni–38Co–YZA (**b**) and Ni–85Co–YZA (**c**) composites

Fig. 4 XRD diffractograms of Ni–YZA (**a**), Ni–17Co–YZA (**b**), Ni–38Co–YZA (**c**) and Ni–85Co–YZA (**d**) coatings

composite is due to the presence of hcp phase as is evident from XRD studies (Fig. 4). Similar reduction in hardness has also been observed for Ni–Co–SiC composites deposited from a high speed sulphamate bath [42].

3.4 Tribological properties

Figure 6 shows the comparative total wear loss of the various coated pins and disc subjected to a dry sliding wear test. A rise in initial wear loss is observed for Ni–YZA and Ni–17Co–YZA coatings. The initial loss for a sliding distance of 700 m and 500 m in Ni–YZA and Ni–17Co–YZA deposits, respectively, is due to the running-in process resulting in an equilibrium surface condition. Further increase in sliding distance has resulted in a condition of like on like wear, generated due to the material transfer (confirmed by Raman spectra) from the pin to the disc and henceforth the displacement in material attained a steady state value. Alloying of the nickel matrix with higher cobalt contents of 38 wt.% and 85 wt.%, has led to a reduction in the initial wear loss. The wear volume loss of Ni–85Co composite is less compared to Ni–17Co and plain Ni composite although it has exhibited reduced microhardness.

to 12 nm). The hardness of Ni–85Co–YZA composite (360 VHN) can be associated with the codeposition of large amount of YZA particles. This is responsible for the particulate strengthening effect, leading to an increased hardness of the composite compared to its alloy (255 VHN). The reduction in hardness of Ni–85Co–YZA
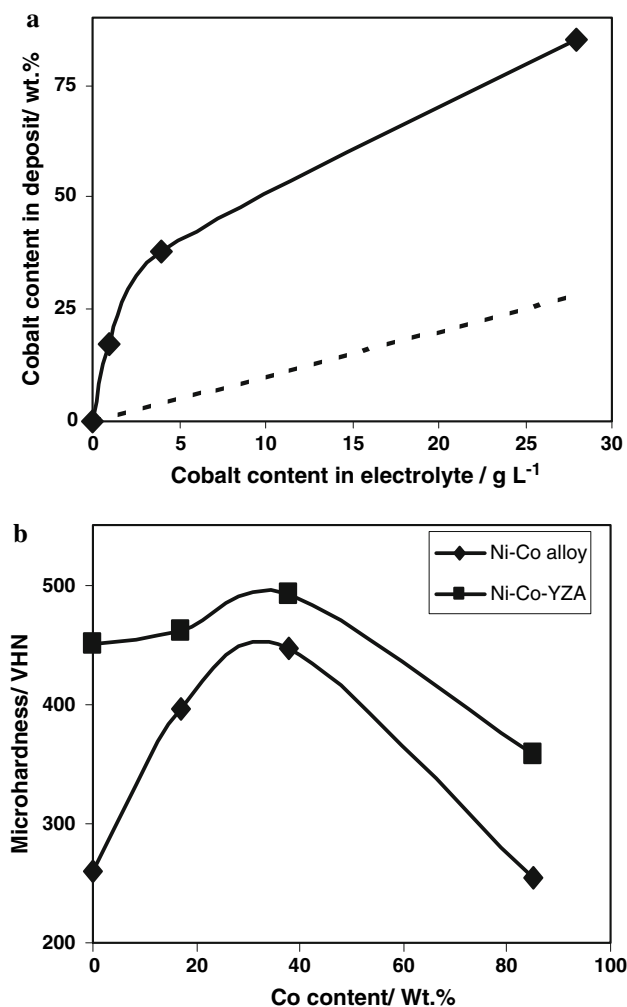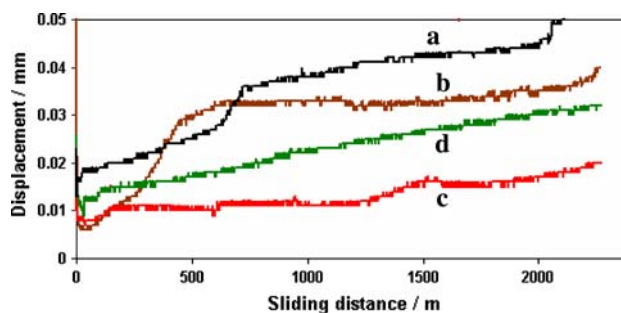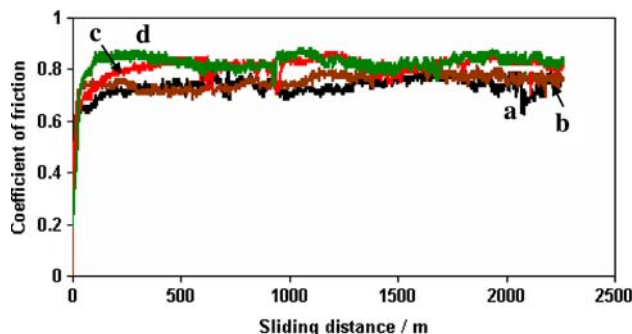
Fig. 5 Ni–Co anomalous codeposition (**a**) and the effect of Co content on the microhardness of Ni–Co alloys/Ni–Co–YZA composites (**b**)

Fig. 6 Comparative total wear loss (from pin and disc) of Ni–YZA (a), Ni–17Co–YZA (b), Ni–38Co–YZA (c) and Ni–85Co–YZA (d) composites

**Fig. 7** Comparative coefficient of friction of Ni–YZA (a), Ni–17Co–YZA (b), Ni–38Co–YZA (c) and Ni–85Co–YZA (d) composites

This can be associated with the presence of the hcp phase. Hence, the wear behaviour depends not only on the hardness but also on the phase structure. Similar behaviour has been observed for Ni–Co–SiC composites [42]. However, Ni–38Co–YZA composite has exhibited the least wear volume loss of all the composites, indicating its best wear performance. This could be due to its higher microhardness. The modulus of elasticity of a material also plays an important role in imparting wear resistance [49]. However,

this aspect has not been dealt with in this paper. The average dynamic coefficient of friction of Ni/Ni–Co–YZA composites are shown in Fig. 7 and also listed in Table 2. Based on the wear coefficient values (Table 2), the type of wear is found to be of an adhesive nature (burnishing/polishing type). It is observed that the Ni–YZA composite exhibited a marginally lower coefficient of friction (COF) value of 0.734 compared to Ni–Co–YZA composites (0.75–0.82).

The nature of wear is identified from the Raman spectrum of the wear tracks on the disc. The spectrum of the wear tracks of various Ni–Co–YZA composite coatings is shown in Fig. 8. The observed bands at wave numbers lower than 1000 cm^{-1} for all composite coatings, are due to the formation of different oxides. The Ni–YZA composite has exhibited characteristic bands at 476 cm^{-1}, 560 cm^{-1} and 692 cm^{-1} corresponding to the presence of NiO (former) and Fe_3O_4 (latter two). Bands at 402 cm^{-1},

Table 2 Comparative wear rates and coefficient of friction of various Ni–Co–YZA composite coatings

Coating	Area fraction of YZA particles	Wear volume loss/mm^3 m^{-1}	Wear coefficient	Coefficient of friction
Ni–YZA	6	1.1106×10^{-5}	5.00×10^{-6}	0.734
Ni–17Co–YZA	4	0.9302×10^{-5}	4.30×10^{-6}	0.755
Ni–38Co–YZA	7	0.1388×10^{-5}	6.83×10^{-7}	0.807
Ni–85Co–YZA	12	0.2777×10^{-5}	9.94×10^{-7}	0.823
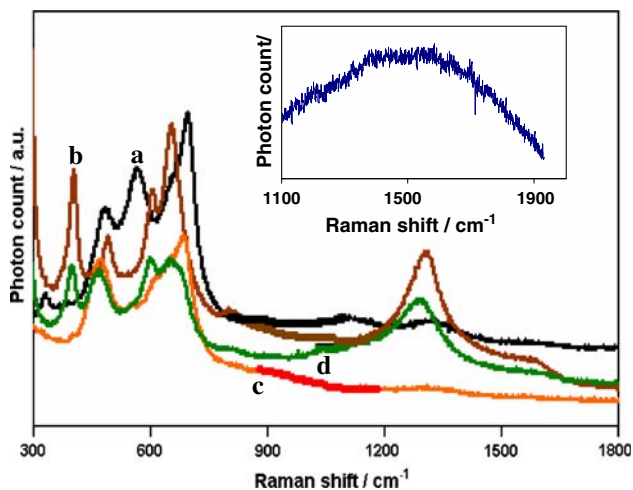
Fig. 8 Comparative Raman spectrum of the wear tracks of Ni–YZA (a), Ni–17Co–YZA (b), Ni–38Co–YZA (c) and Ni–85Co–YZA (d) composite coatings; insert shows the spectrum of as-synthesized YZA particles

487 cm^{-1}, 603 cm^{-1} and 651 cm^{-1} are observed for Ni–17Co–YZA coating. These bands are due to the presence of αFe_2O_3, NiO, Co_3O_4 and $NiCo_2O_4$ respectively [50, 51]. Ni–38Co–YZA coating exhibited characteristic bands corresponding to the formation of cobalt oxides namely Co_3O_4 and CoO at 472 cm^{-1} and 690 cm^{-1}. Characteristic bands are observed at 396 cm^{-1}, 463 cm^{-1}, 596 cm^{-1} and 644 cm^{-1} on the wear track of Ni–85Co–YZA. These can be associated to the presence of αFe_2O_3, Co_3O_4, Co_3O_4 and $NiCo_2O_4$ oxides. Bands at higher wave numbers of 1304 cm^{-1}, 1299 cm^{-1} and 1281 cm^{-1} are also observed for Ni–YZA, Ni–17Co–YZA and Ni–85Co–YZA composites, respectively. This corresponds to the broad band exhibited by the synthesised YZA particulates (insert Fig. 8), thereby revealing the presence of YZA on the wear track. The presence of oxides of Ni, Co and YZA particles on the wear track depicts the transfer of material (under dry sliding conditions) from the pin to the disc affirming the nature of wear to be adhesive.

3.5 Corrosion behaviour

The corrosion rate of the various YZA coatings studied using the weight loss method is listed in Table 3. Ni–YZA and Ni–17Co–YZA composites displayed reduced corrosion compared to Ni–38Co–YZA and Ni–85Co–YZA coatings. The least rate is observed for Ni–17Co–YZA composite. Thus, it can be inferred that the presence of 17 wt.% cobalt is optimum for improving the corrosion behaviour of the composites. A similar observation has also been made for Ni–Co alloys [40]. The SEM analysis of the corroded surface is shown in Fig. 9. The alumina rich particles (Table 4)

Table 3 Corrosion rates of various Ni–Co–YZA composites

Coating	Corrosion rate/mpy
Pure Ni	0.55958
Ni–YZA	0.39970
Ni–17Co–YZA	0.27979
Ni–38Co–YZA	1.27904
Ni–85Co–YZA	2.23832
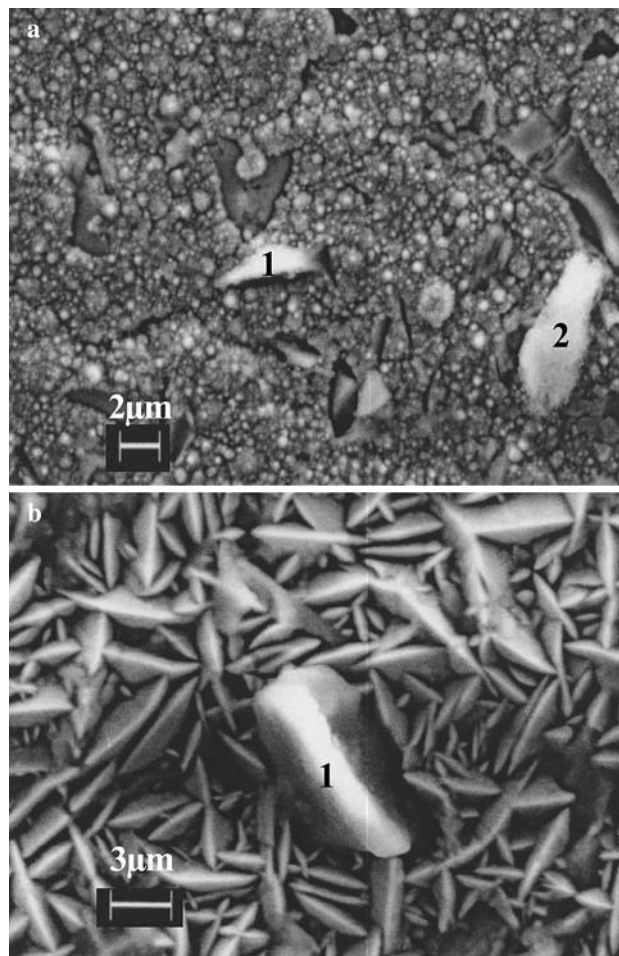
Fig. 9 Surface morphology of corroded Ni–38Co–YZA (**a**) and Ni–85Co–YZA (**b**) composites revealing the Al_2O_3 rich particle

which appeared filamental prior to corrosion studies were exposed to a greater extent after the immersion in the corrosive medium. This is clear from the difference in the extent of brightness of the particle as shown in Figs. 9a,b and 3b,c. This may be either due to the uniform dissolution of the deposits or accelerated corrosion at the matrix–particle interface. Detailed studies are required to understand this observation. It is evident from the EDX studies that the oxygen content had increased after the immersion in 3.5%

Table 4 EDX analysis of the Al$_2$O$_3$ rich particle in corroded Ni–38Co–YZA and Ni–85Co–YZA composite coating

Element	Ni–38Co–YZA (wt.%)	Ni–85Co–YZA (wt.%)
O	40	39
Al	17	13
Co	14	31
Ni	22	3
Y	1	4
Zr	7	10

Table 5 EDX analysis of the as deposited and corroded matrix of Ni–38Co–YZA and Ni–85Co–YZA composites

Element	Ni–38Co–YZA wt.%		Ni–85Co–YZA wt.%	
	As-deposited	Corroded	As-deposited	Corroded
O	1	6	5	11
Co	37	20	87	79
Ni	62	74	7	8

Fig. 10 Effect of heat treatment on microhardness of the coatings: Ni (a[1]), Ni–YZA (a), Ni–17Co (b[1]), Ni–17Co–YZA (b), Ni–38Co (c[1]), Ni–38Co–YZA (c), Ni–85Co (d[1]), Ni–85Co–YZA (d)
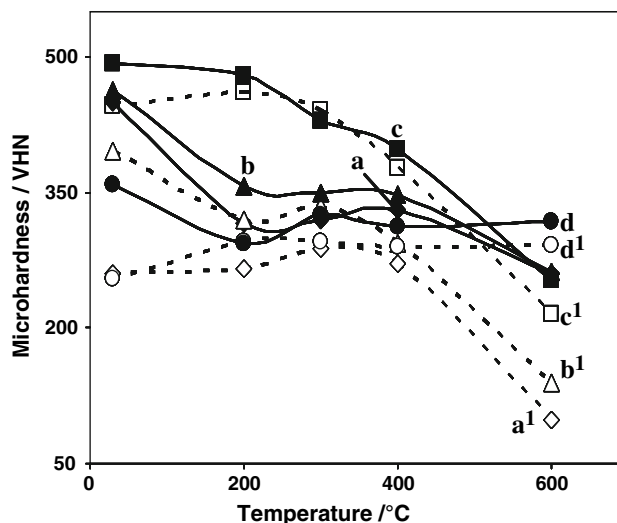
NaCl (Table 5). This can be linked with the fact that the anions present in the solution are Cl$^-$ and OH$^-$. These ions react with the metals to form chloride and hydroxide compounds. The chlorides are highly soluble hence the hydroxides can contribute to the increase in oxygen content. Further, Co has greater susceptibility to form oxide and thus the oxygen content is higher in Ni–85Co–YZA composite compared to Ni–38Co–YZA composite (Table 5).

3.6 Thermal stability

The microhardness of Ni, Ni–Co alloys and their YZA composites subjected to heat treatment is indicated in Fig. 10. Plain Ni shows a drastic reduction in hardness from 260 VHN to 99 VHN beyond 400 °C. A similar trend has been observed on alloying with 17 wt.% Co and 38 wt.% Co, however, the hardness attained was higher i.e.140 VHN and 215 VHN respectively. The reduction in microhardness with the addition of 85 wt.% Co is negligible (255 VHN to 290 VHN). This shows that although Co rich alloy possesses low microhardness it is more thermally stable compared to Ni rich alloy. These observations also hold good for the YZA composite coatings. Similar behaviour has been reported for plain cobalt coatings by Safranek [28]. Thus by varying the cobalt content, composite coatings can be tailored to suit various applications.

4 Conclusions

An attempt has been made to develop an economical coating that has improved thermal stability. Yttria

stabilised zirconia/alumina composite (YZA) powder was codeposited in Ni–Co alloy matrix. The cobalt content in the matrix was varied and the effect of reinforcement was related to the mechanical, chemical and thermal properties. The YZA particles did not change the surface morphology of the various Ni–Co alloys, although, particles of various shape, size and composition were incorporated. Also, it did not affect the phase structure of the alloys. The EDX studies revealed that a change in composition occurred in the YZA particles compared to the as-prepared condition. In the electrodeposited coatings zirconia rich particles were blocky, while the alumina rich were filamental and flaky. From the image analysis, no substantial variation in the particle incorporation occurred except for the Ni–85Co alloy, where higher incorporation was observed. The microhardness studies of the composites showed an enhancement in the values in comparison with that of the alloys. Thus, YZA incorporation not only improves the hardness but also enhances the wear resistance. The corrosion studies revealed that Ni–17Co–YZA composite exhibited the best corrosion resistance compared to the others. Thus by varying the cobalt content, the composite coatings can be tailored for different applications. In a corrosive atmosphere, where moderate wear resistance is required Ni–17Co–YZA composite is preferred. Ni–38Co–YZA composite coatings can be used in applications where moderate corrosion resistance and high wear resistance is necessary. Further, in applications where the microhardness variation with reference to high temperatures (600 °C) should be minimum, use of composite coating containing 85 wt.% Co is suggested.

References

1. Thoma M (1985) 4th international tribology symposium–eurotrib 85, Lyon
2. Greco VP, Baldauf W (1968) Plating 250
3. Pushpavanam M, Varadajan G, Krishnamurthy S, Shenoi BA (1974) Electroplat Met Finish 10
4. Celis JP, Roos JR (1982) Coat Corros 5:1
5. Brooman EW (2006) J Appl Surf Finish 1:38
6. Kuo S-L (2005) J Chin Inst Eng 28:1
7. Nowak P, Socha RP, Kaisheva M et al (2000) J Appl Electrochem 30:429
8. Wang S-C, Wei W-CJ (2003) J Mater Res 18:7
9. Shawki S, Abdel Hamid Z (1997) Aircr Eng Aerosp Technol 69:432
10. Socha RP, Nowak P, Laajalehto K, Vayrynen J (2004) Colloids Surf A: Physicochem Eng Aspects 235:45
11. Lampke Th, Leopold A, Dietrich D et al (2006) Surf Coat Technol 201:3510
12. Qu NS, Zhu D, Chan KC (2006) Scr Mater 54:1421
13. Xue Y-J, Li J-S, Ma W et al (2006) J Mater Sci 41:1781
14. Benea L, Lakatos-Varsanyi M, Maurin G (II-2003) The Annals of Dunarea De Jos University of Galati, Fascicle IX Metallurgy and Materials Science, ISSN 1453-083X NR
15. Moller A, Hahn H (1999) Nanostruct Mater 12:259
16. Hou F, Wang W, Guo H (2006) Appl Surf Sci 252:3812
17. Wang W, Hou F-Y, Wang H, Guo H-T (2005) Scr Mater 53:613
18. Wang W, Guo HT, Gao JP et al (2000) J Mater Sci 35:1495
19. Rajiv EP, Annamalai VE, Seshadri SK (1992) J Mater Sci Lett 11:466
20. Balathandan S, Annamalai VE, Seshadri SK (1992) J Mater Sci Lett 11:449
21. Jun L, Yiyong W, Dianlong W, Xinguo H (2000) J Mater Sci 35:1751
22. Aruna ST, Rajam KS (2003) Scr Mater 48:507
23. Choi SR, Bansal NP (2005) Ceram Int 31:39
24. Sharif AA, Mecartney ML (2004) J Eur Ceram Soc 24:2041
25. Mangalaraja RV, Chandrasekhar BK, Manohar P (2003) Mater Sci Eng A 343:71
26. Lu XJ, Xiao P (2007) J Eur Ceram Soc 27:2613
27. Dini JW, Johnson HR, Helms JR (1972) Sandia livermore laboratories report No. SCL-DR-720090
28. Safranek WH (1974) The properties of electrodeposited metals and alloys—a handbook. American Elsevier Publishing Company, Inc
29. Wang L, Gao Y, Xue Q, Liu H, Xu T (2005) Appl Surf Sci 242:326
30. Vicenzo A, Cavallotti PL (2004) Electrochim Acta 49:4079
31. Brenner A (1963) Electrodeposition of alloys—principles and practice, vol II. Academic Press NY
32. Golodnitsky D, Gudin NV, Volyanuk GA (1998) Plat Surf Finish 2:65
33. Malone GA, Winkelman M (1989) High performance alloy electroforming final report No. 8874-927001
34. Golodnitsky D, Gudin NV, Volyanuk GA (2000) J Electrochem Soc 147:4156
35. Golodnitsky D, Rosenberg Yu, Ulus A (2002) Electrochim Acta 47:2707
36. Fan CL, Piron DL (1996) Electrochim Acta 41:10:1713
37. Qiao G, Jing T, Wang N et al (2005) Electrochim Acta 51:85
38. Wu BYC, Ferreira PJ, Schuh CA (2005) Metall Mater Trans A 36A:1927
39. Bai A, Hu C-C (2002) Electrochim Acta 47:3447
40. Srivastava M, Ezhil Selvi V, William Grips VK, Rajam KS (2006) Surf Coat Technol 201:3051
41. Klug H, Alexander L (1974) X-ray diffraction procedures for polycrystalline and amorphous materials. John Wiley, New York
42. Srivastava M, William Grips VK, Rajam KS (2007) Appl Surf Sci 253:3814
43. Archard JF (1953) J Appl Phys 24:981
44. http://www.alspi.com/coupons(intro).pdf
45. Wearmouth WR (1982) Trans Inst Metal Finish 60:68
46. Walter RJ (1986) Plat Surf Finish 48
47. Srinivasan D, Chattopadhayay K (2004) Mater Sci Eng A 375:1228
48. Zimmerman AF, Palumbo G, Aust KT, Erb U (2002) Mater Sci Eng A 328:137
49. Ni W, Cheng Y-T, Lukitsch MJ et al (2004) Appl Phys Lett 85:4028
50. Windisch CF Jr, Ferris KF, Exarhos GF (2001) J Vac Sci Technol A 19
51. Simionato M, Moreira Assaf E (2003) Mater Res 6:535